Peer reviewed version

Link to published version (if available):
10.1080/14786435.2015.1040480

Link to publication record in Explore Bristol Research
PDF-document

University of Bristol - Explore Bristol Research
General rights

Electron-phonon superconductivity in BaSn$_5$

D. Ernsting,[1] T.E. Millichamp,[1] and S.B. Dugdale[1]

[1]*H.H. Wills Physics Laboratory, University of Bristol,*
Tyndall Avenue, Bristol, BS8 1TL, United Kingdom

First-principles calculations of the electronic structure and phonon dispersion relation of the superconducting compound BaSn$_5$ were performed. This has allowed the calculation of the electron-phonon matrix elements from which the electron-phonon coupling constant was found to be $\lambda_{\mathrm{ep}} = 0.87$. Application of the Allen–Dynes formula with $\mu^* = 0.11$ yielded a superconducting transition temperature of $T_c = 4.2$ K. The calculated T_c agrees well with the available experimental data and indicates that BaSn$_5$ is an electron-phonon superconductor with intermediate strength electron-phonon coupling.

INTRODUCTION

Very recently, superconductivity was discovered in the H$_2$S system with a record superconducting critical temperature of $T_c = 190$ K under 200 GPa of hydrostatic pressure [1]. The strong isotope shift of T_c in D$_2$S relative to H$_2$S evidences the major role of phonons in the superconductivity. This has lead to a renewed interest in studies of conventional (electron-phonon) superconductors, especially in systems where the electrons couple to special phonon modes, *i.e.* modes for which the electron-phonon coupling is particularly strong. The focus of this study is not on superconductors for which T_c is large but, rather, on systems where the coupling of electrons to special phonon modes is important.

The previous T_c record for a phonon-mediated superconductor was held by the multiband superconductor MgB$_2$ with $T_c \approx 40$ K at ambient pressure [2]. Since many material properties are related to the symmetry and chemical environment of the constituent atoms, insights into these compounds can be gained by studying structural and chemical analogues. MgB$_2$ has the AlB$_2$ structure which belongs to the $P6/mmm$ space group. Another member of this space group is BaSn$_5$, the Sn-richest phase in the Ba-Sn intermetallic series whose structure has only recently been solved (see Figure 1) [3]. BaSn$_5$ also has a superconducting phase below $T_c = 4.4$ K [3, 4]. Recently, Lin *et al.* have grown high-quality single-crystal samples of BaSn$_5$ and characterised its thermodynamic and transport properties in both the normal and superconducting phases [4]. Although the band structure and density-of-states (DOS) of BaSn$_5$ have been calculated previously [3], no calculations have been reported for the Fermi surface, phonon dispersion relation or electron-phonon coupling. The aim of this study is to understand the role of electron-phonon coupling in the superconductivity of this compound.

The ground state electronic structure in the normal phase was calculated using a highly accurate full-potential augmented plane-wave plus local orbital (FP-APW+lo) method. In order to investigate phonon mediated superconductivity, a plane-wave pseudopotential
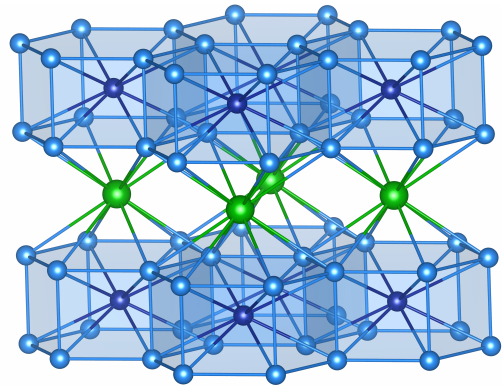

FIG. 1: Crystal structure of BaSn$_5$. The Ba atoms are green, Sn1 atoms are dark blue and Sn2 atoms are light blue.

TABLE I: Experimental lattice constants [4] and atomic Wyckoff positions [3] of BaSn$_5$.

BaSn$_5$ lattice constants [4]		
a [Å]		5.368(4)
c [Å]		7.097(4)
c/a		1.322(1)
BaSn$_5$ Wyckoff positions [3]		
Atom	x	y	z
Ba	0	0	1/2
Sn1	0	0	0
Sn2	2/3	1/3	0.2085(1)

method was used to calculate the phonon dispersion relation by linear response and to evaluate the strength of the electron-phonon coupling. From these calculations, it is shown that the electron-phonon coupling in this compound is of intermediate strength and is able to support the observed superconductivity.

ELECTRONIC STRUCTURE

The particular implementation of the FP-APW+lo method used to determine the ground state electronic
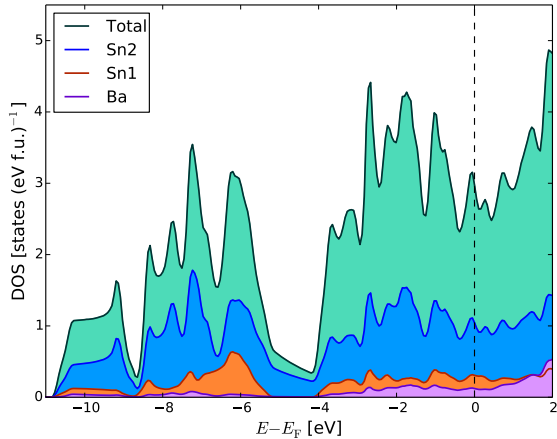
FIG. 2: Total and site-projected DOS of BaSn$_5$. The total DOS is green, Ba DOS is purple, Sn1 DOS is orange and Sn2 DOS is blue. The interstitial DOS is not plotted.
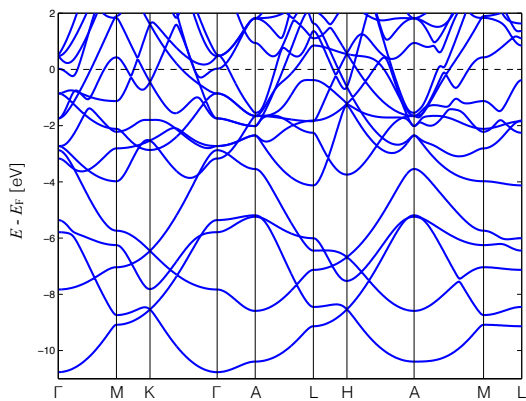

FIG. 3: Band structure of BaSn$_5$ along selected high-symmetry directions.

structure was the ELK code [5]. The experimental lattice constants and internal atomic coordinates were used in the calculation (see Table I) [3, 4]. The muffin-tin radii for Ba, Sn1 and Sn2 were 2.8000, 2.6000 and 2.6000 a.u., respectively, and, in the interstitial region, the plane-wave cutoff was determined by $|\boldsymbol{G} + \boldsymbol{k}|_{\mathrm{max}} = 8.0/R_{\mathrm{mt}}$, where R_{mt} is the average muffin-tin radius. Convergence was achieved with 4096 $\boldsymbol{k}$-points in the irreducible Brillouin zone using the Perdew–Wang-91 generalised gradient approximation (PW91-GGA) [6, 7] to the exchange-correlation functional.

The calculated DOS is shown in Figure 2. At the Fermi level, E_{F}, the primary contribution to the DOS is from hybridised Sn2 s and p-states. There is also a further contribution from Sn1 p-states and a small contribution from Ba d-states. The Sn2 atoms contribute more states at E_{F} than the Sn1 atoms. In BaSn$_5$, the calculated
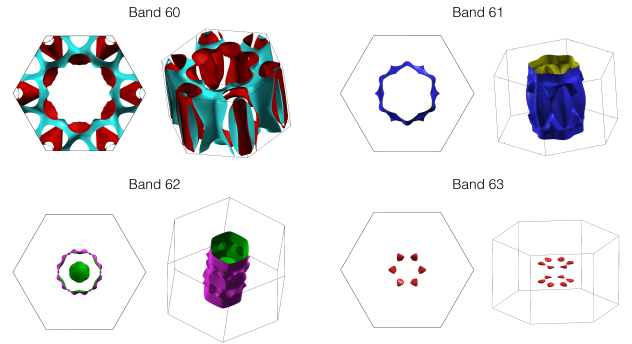

FIG. 4: The four Fermi surface sheets of BaSn$_5$ viewed down the c^*-axis (left) and various low-symmetry directions (right) for clarity.

DOS at the Fermi level was $N(E_{\mathrm{F}}) = 2.98$ states (eV f.u.)$^{-1}$. Lin $et\ al.$ state that the pressure derivative of T_c, $\mathrm{d}T_c/\mathrm{d}P \approx -0.053 \pm 0.001$ K/kbar, is rather small and suggest that this is possibly the result of a weak energy dependence of $N(E_{\mathrm{F}})$ [4]. In contrast, we find E_{F} to lie just above a local maximum in the DOS, in agreement with the previous calculation [3].

The calculated band structure is shown Figure 3 and shows that four bands cross E_{F}. The corresponding Fermi surface sheets are shown in Figure 4. The first sheet (band 60) has a rather complicated web-like topology. The second sheet (band 61) is a highly-distorted tube centered at the Γ-point with a rounded hexagonal cross-section. The third sheet (band 62) is also centered at the Γ-point and consists of two parts; another highly warped tube with a rounded hexagonal cross-section and a 'dumbell'-shaped sheet with its axis aligned along the c^*-axis. The fourth sheet (band 63) consists of 12 rounded triangular-shaped segments.

Lin $et\ al.$ measured the dc magnetisation as a function of applied magnetic field along the c-axis and were able to resolve two de Haas–van Alphen (dHvA) frequencies of 0.116 kT (α) and 0.159 kT (β). By measuring the temperature dependence of their amplitudes and applying the Lifshitz-Kosevich equation, they were able to extract effective masses of $m_\alpha = 0.09m_e$ and $m_\beta = 0.13m_e$ where m_e is the free electron rest mass [4]. In order to make a comparison with experiment, the predicted dHvA frequencies were calculated from our calculated electronic structure using the SKEAF code [8]. The calculated frequencies are shown in Figure 5 for various magnetic field directions. We find three extremal orbits on band 60 (for the magnetic field aligned parallel to the c-axis) with frequencies close to those measured by Lin $et\ al.$. The frequencies were 0.051 kT, 0.186 kT and 0.218 kT and the effective masses were $0.061m_e$, $0.090m_e$ and $0.076m_e$, respectively. In order to improve the agreement between theory and experiment and to determine which extremal orbits to compare with those of Lin $et\ al.$, band 60 was
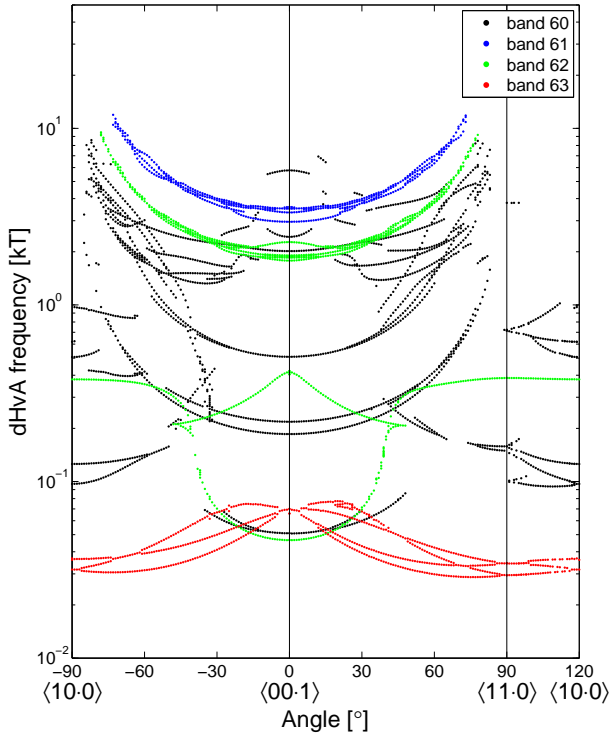
FIG. 5: Predicted angular dependences of the calculated dHvA frequencies for BaSn$_5$.

rigidly shifted up by 7 mRy relative to E_F. The frequencies of the three extremal orbits were now 0.118 kT, 0.149 kT and 0.160 kT with effective masses of $0.073m_e$, $0.058m_e$ and $0.065m_e$, respectively. Rigidly shifting the calculated bands with respect to E_F in order to bring the predicted extremal areas into agreement with experiment has become quite a common practice [9], particularly in the iron-pnictide superconductors [10–12]. The shift required here is smaller than those required for the iron-pnictides which is perhaps not surprising considering that the electronic correlations in BaSn$_5$ are expected to be smaller.

In the electronic structure calculation, many-body effects are explicitly neglected. These effects increase the experimental linear electronic specific heat coefficient, γ^exp, relative to that calculated, γ^calc. The ratio of γ^exp to γ^calc allows us to estimate the mass renormalisation, λ, through the relationship,

$$\frac{\gamma^\mathrm{exp}}{\gamma^\mathrm{calc}} = 1 + \lambda. \qquad (1)$$

Lin *et al.* experimentally determined $\gamma^\mathrm{exp} = 10.8$ mJ K^{-2} mol^{-1} [4] and γ^calc is given by,

$$\gamma^\mathrm{calc} = \frac{\pi^2}{3} k_\mathrm{B}^2 N(E_\mathrm{F}), \qquad (2)$$

giving $\gamma^\mathrm{calc} = 7.00$ mJ K^{-2} mol^{-1}, implying $\lambda \approx$

0.54. If electron-phonon coupling is assumed to dominate the mass renormalisation (and explicitly neglecting other mechanisms), the electron-phonon coupling constant, λ_ep, can be set equal to the mass renormalisation. For $\lambda_\mathrm{ep} < 1.5$, it is possible to estimate T_c from the McMillan equation [13],

$$T_c = \frac{\Theta_\mathrm{D}}{1.45} \exp\left(\frac{-1.04(1+\lambda_\mathrm{ep})}{\lambda_\mathrm{ep} - \mu^*(1+0.62\lambda_\mathrm{ep})}\right), \qquad (3)$$

where Θ_D is the Debye temperature and μ^* represents a (dimensionless) Coulomb pseudopotential, which characterises the strength of the (screened) electron-electron Coulomb repulsion. Using our estimated $\lambda_\mathrm{ep} \approx 0.54$, the experimentally determined $\Theta_\mathrm{D} = 182.5$ K from Lin *et al.* [4] and choosing values of μ^* between 0.10–0.15 (values between 0.1–0.2 are considered physically reasonable [14, 15], but values between 0.10–0.15 are more common [9, 16]), we estimate $T_c \approx 1.1$–2.5 K which is much smaller than the experimentally observed value of $T_c = 4.4$ K [3, 4]. By solving Eq. 3 for λ_ep with the experimentally determined Θ_D and T_c, we can instead expect $\lambda_\mathrm{ep} \approx 0.65$–0.77 for values of μ^* between 0.10–0.15. Given that the expected λ_ep is higher than that estimated from the ratio of experimental and calculated specific heats, it seems likely that the observed superconductivity may result from the coupling of electrons to special phonon modes.

ELECTRON-PHONON COUPLING

The particular implementation of the plane-wave pseudopotential method used to calculate the phonon dispersion relation and electron-phonon coupling was the the Quantum Espresso code [17]. The chosen pseudopotentials were ultrasoft scalar relativistic and convergence was checked with respect to both the plane-wave cutoffs and $\boldsymbol{k}$-point density. The phonon dynamical matrices were calculated on an $8 \times 8 \times 8$ $\boldsymbol{q}$-point mesh with Brillouin zone integrations on a $16 \times 16 \times 16$ $\boldsymbol{k}$-point mesh and wavefunction and charge density cutoffs of 40 Ry and 400 Ry, respectively. Since the accurate evaluation of the electron-phonon matrix elements requires a very dense sampling of the Brillouin zone, these were evaluated on a $32 \times 32 \times 32$ $\boldsymbol{k}$-point mesh. Again, the PW91-GGA functional [6, 7] was chosen to treat exchange and correlation. In order to have confidence in a pseudopotential calculation, it is also important to check that the calculated electronic structure is consistent with full-potential calculations. The calculated band structure and DOS were therefore checked against our FP-APW+lo calculation and were barely distinguishable.

The calculated phonon dispersion of BaSn$_5$ is shown in Figure 6. Here, the size of the points indicates the relative size of the mode, ν, and $\boldsymbol{q}$-point resolved phonon linewidth, $\gamma_{\boldsymbol{q}\nu}$, (inverse phonon lifetime). In BaSn$_5$, the
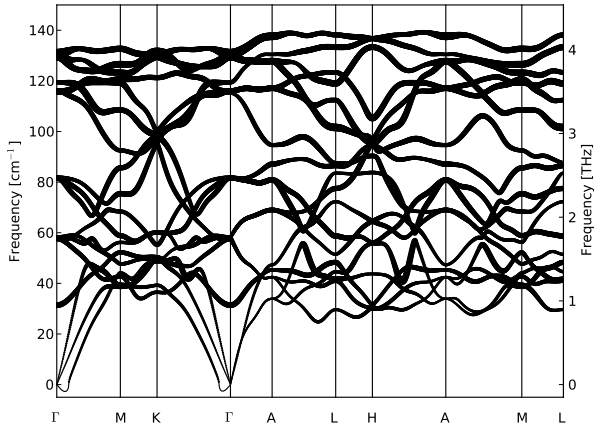
FIG. 6: Phonon dispersion of BaSn$_5$ along selected high-symmetry directions. The size of the points indicates the relative size of the phonon linewidth of that mode at that q-point.
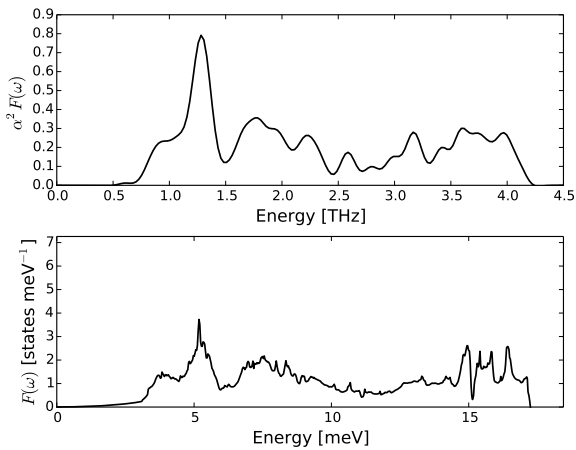

FIG. 7: Eliashberg function, $\alpha^2 F(\omega)$, (top) and phonon DOS, $F(\omega)$, (bottom) of BaSn$_5$. As 1 THz is equivalent to 4.1 meV (or 33 cm^{-1}), the ranges spanned by the two separate plots are equivalent.
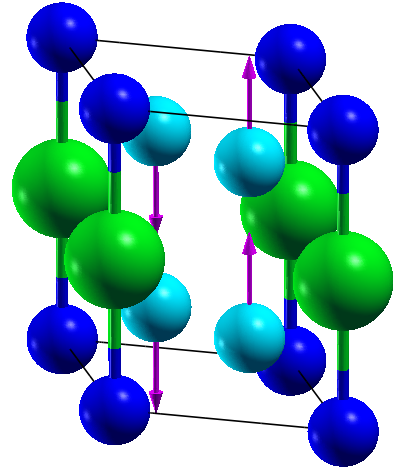

FIG. 8: Displacement pattern for the lowest optical phonon mode (mode 4). The symmetry of this mode is E_{2g} and it is a shear-type mode. The Ba atoms are green, Sn1 atoms are dark blue and Sn2 atoms are light blue. The atomic displacements are indicated by the purple arrows and the size of the arrows are proportional to the displacement. The size of the arrows have been greatly exaggerated for clarity.

frequency of the lowest acoustic phonon mode becomes imaginary (shown as negative in Figure 6) between the Γ-point and one quarter of the distance towards the M-point and similarly between the Γ-point and one quarter of the distance towards K-point of the hexagonal Brillouin zone. This is probably because of a numerical instability due to the size of the plane-wave cutoff that is required for accurate numerical convergence near the Γ-point when using ultrasoft pseudopotentials with GGA exchange-correlation functionals. It is also worth considering that, in the calculation, the translational symmetry of the crystal is broken because of the discreteness of the fast Fourier transform grid. This leads to acoustic phonon modes with non-zero frequency at the Γ-point. In

order to restore the translational invariance of the crystal, the acoustic sum rule (ASR) is imposed, thereby forcing the acoustic phonon modes to have zero frequency at the Γ-point. Direct diagonalisation of the dynamical matrix at the Γ-point gives an imaginary frequency of 0.14i THz for the lowest two acoustic phonon modes and the ASR then forces these modes to zero frequency at the Γ-point. In order to check whether this was a real lattice instability, the plane-wave pseudopotential calculation was repeated with wavefunction and charge density cutoffs and 80 Ry and 800 Ry, respectively. Unfortunately, calculating the dynamical matrices throughout the Brillouin zone with the larger cutoffs is computationally impractical. It is, however, possible to calculate the dynamical matrix at the Γ-point with the larger cutoffs. Direct diagonalisation of the dynamical matrix at the Γ-point yielded a real frequency of 0.17 THz for the lowest two acoustic phonon modes. For the optical phonon modes, the largest frequency differences were less than 5% of the calculation with the smaller cutoffs and most of the differences were significantly smaller than this. It therefore seems likely that the imaginary phonon frequencies in Figure 6 are due to a numerical instability near the Γ-point rather than a lattice instability.

Both the calculated phonon density of states $F(\omega)$ and Eliashberg function $\alpha^2 F(\omega)$ are shown in Figure 7. This yields an electron-phonon coupling constant of $\lambda_{\text{ep}} = 0.87$. In BaSn$_5$, the average coupling across all 18 phonon modes is 0.0483, however, the couplings to the first five modes are much stronger (0.0951, 0.0769, 0.0942, 0.1051

and 0.0913, respectively). These first five modes are responsible for the large peak in $\alpha^2 F(\omega)$ around 1.25 THz and contribute more than half of the total λ_{ep}. It is worth noting that the mode, ν, and q-point resolved electron-phonon couplings, $\lambda_{q\nu}^{ep}$, are set to zero for the phonons with imaginary frequencies. The atomic displacement pattern for the lowest optical phonon mode (mode 4) is shown in Figure 8. The symmetry of this mode is E_{2g} and it is a shear-type mode. This mode has the largest electron-phonon coupling and involves c-axis oscillations of the Sn2 atoms with adjacent in-plane Sn2 atoms oscillating out-of-phase and adjacent out-of-plane Sn2 atoms oscillating in-phase.

After calculating λ_{ep}, and determining the logarithmically averaged phonon frequency, ω_{log}, the superconducting critical temperature can be estimated from the Allen–Dynes formula [18],

$$T_c = \frac{\hbar\omega_{log}}{1.2k_B} \exp\left(\frac{-1.04(1+\lambda_{ep})}{\lambda_{ep} - \mu^*(1+0.62\lambda_{ep})}\right). \quad (4)$$

Using the calculated $\lambda_{ep} = 0.87$, $\omega_{log} = 57.10$ cm^{-1}, and choosing values of μ^* between 0.10–0.15, T_c is found to lie between 3.3–4.5 K. Choosing $\mu^* = 0.11$ yields $T_c = 4.2$ K which agrees remarkably well with the experimentally observed value of $T_c = 4.4$ K [3, 4].

CONCLUSION

In conclusion, the electronic structure and phonon dispersion relation of BaSn$_5$ were calculated from first-principles. This allowed an evaluation of the electron-phonon coupling from which the superconducting critical temperature was estimated. The electron-phonon coupling constant was found to be $\lambda_{ep} = 0.87$ and application of the Allen–Dynes formula with Coulomb pseudopotential of $\mu^* = 0.11$ yielded a superconducting critical temperature of $T_c = 4.2$ K, in excellent agreement with the experimentally observed value of $T_c = 4.4$ K [3, 4]. Finally, the calculations show that the main contribution to the electron-phonon coupling comes from the low energy phonon modes.

Acknowledgements

[1] A.P. Drozdov, M.I. Eremets and I.A. Troyan, arXiv:1412.0460 (unpublished) (2014).

[2] J. Nagamatsu, N. Nakagawa, T. Muranaka, Y. Zenitani and J. Akimitsu, Nature 410 (2001) p. 63.

[3] T.F. Fässler, S. Hoffmann and C. Kronseder, Zeitschrift für anorganische und allgemeine Chemie 627 (2001) p. 2486.

[4] X. Lin, S.L. Bud'ko and P.C. Canfield, Philosophical Magazine 92 (2012) p. 3006.

[5] K. Dewhurst, S. Sharma and C. Ambrosch-Draxl, ELK FP-LAPW Code; Available at http://elk.sourceforge.net.

[6] J.P. Perdew, J.A. Chevary, S.H. Vosko, K.A. Jackson, M.R. Pederson, D.J. Singh and C. Fiolhais, Phys. Rev. B 46 (1992) p. 6671.

[7] J.P. Perdew, J.A. Chevary, S.H. Vosko, K.A. Jackson, M.R. Pederson, D.J. Singh and C. Fiolhais, Phys. Rev. B 48 (1993) p. 4978.

[8] P.M.C. Rourke and S.R. Julian, Computer Physics Communications 183 (2012) p. 324.

[9] D. Billington, T.M. Llewellyn-Jones, G. Maroso and S.B. Dugdale, Superconductor Science and Technology 26 (2013) p. 085007.

[10] L. Ortenzi, E. Cappelluti, L. Benfatto and L. Pietronero, Phys. Rev. Lett. 103 (2009) p. 046404.

[11] C. Utfeld, J. Laverock, T.D. Haynes, S.B. Dugdale, J.A. Duffy, M.W. Butchers, J.W. Taylor, S.R. Giblin, J.G. Analytis, J.H. Chu, I.R. Fisher, M. Itou and Y. Sakurai, Phys. Rev. B 81 (2010) p. 064509.

[12] B.J. Arnold, S. Kasahara, A.I. Coldea, T. Terashima, Y. Matsuda, T. Shibauchi and A. Carrington, Phys. Rev. B 83 (2011) p. 220504.

[13] W.L. McMillan, Phys. Rev. 167 (1968) p. 331.

[14] J.P. Carbotte, Rev. Mod. Phys. 62 (1990) p. 1027.

[15] D. Daghero, M. Tortello, G. Ummarino, J.C. Griveau, E. Colineau, R. Eloirdi, A. Shick, J. Kolorenc and R. Lichtenstein A.I. Caciuffo, Nat. Commun. 3 (2012).

[16] D. Billington, S.A.C. Nickau, T. Farley, J.R. Ward, R.F. Sperring, T.E. Millichamp, D. Ernsting and S.B. Dugdale, Journal of the Physical Society of Japan 83 (2014) p. 044710.

[17] P. Giannozzi, S. Baroni, N. Bonini, M. Calandra, R. Car, C. Cavazzoni, D. Ceresoli, G.L. Chiarotti, M. Cococcioni, I. Dabo, A.D. Corso, S. de Gironcoli, S. Fabris, G. Fratesi, R. Gebauer, U. Gerstmann, C. Gougoussis, A. Kokalj, M. Lazzeri, L. Martin-Samos, N. Marzari, F. Mauri, R. Mazzarello, S. Paolini, A. Pasquarello, L. Paulatto, C. Sbraccia, S. Scandolo, G. Sclauzero, A.P. Seitsonen, A. Smogunov, P. Umari and R.M. Wentzcovitch, Journal of Physics: Condensed Matter 21 (2009) p. 395502.

[18] P.B. Allen and R.C. Dynes, Journal of Physics C: Solid State Physics 8 (1975) p. L158.